*Int. J. Electrochem. Sci.*, 14 **(2019)** 11189 – 11198, doi: 10.20964/2019.12.61

International Journal of
ELECTROCHEMICAL
SCIENCE
www.electrochemsci.org

*Short Communication*

# $FeMoO_4$ Nanoprism Supported on Nickel Foam as Electrocatalyst for Oxygen Evolution Reaction

*Jun Nan*[1,2,*], *Min Yang*[1], *Zhengyin Fan*[1], *Xinyao Chen*[1], *Yuanhang Shan*[1]

[1] State Key Laboratory of Heavy Oil Processing, China University of Petroleum (East China), Qingdao 266580, PR China
[2] CenerTech Tianjin Chemical Research and Design Institute Co. Ltd, Tianjin 300131, PR China
[*]E-mail: nanjun@cnooc.com.cn

*Received:* 4 June 2019 / *Accepted:* 24 August 2019 / *Published:* 29 October 2019

Developing electrocatalyst with high efficiency and low cost for oxygen evolution reaction (OER) is of paramount importance to explore sustainable energy technologies. In this work, bimetallic $FeMoO_4$ nanoprism supported on nickel foam is synthesized through a simple one-step hydrothermal method. The optimal molar ratio of molybdenum to iron (1:1) of $FeMoO_4$ is investigated for OER. Benefiting from unique nanoprism structure, fast transmission of electrons or ions, rich exposure of surface active sites, and excellent conductivity enhanced by the substrate of nickel foam (NF), $FeMoO_4$-1/NF electrode exhibits excellent electrocatalytic performance with an overpotential of 284 mV to reach 100 mA $cm^{-2}$ in 1.0 M KOH. This work provides a promising strategy for water oxidation in alkaline solution.

**Keywords:** $FeMoO_4$; bimetallic; nanoprism; nickel foam; oxygen evolution reaction

## 1. INTRODUCTION

Over the past decade years, people have been looking for clean energy to replace fossil fuels [1-4]. Hydrogen is demonstrated as an ideal choice owing the green, renewable, friendly nature [5-8]. Water electrolysis technology provides an effective way for hydrogen generation. However, oxygen evolution reaction (OER) as the anode reaction of water electrolysis is a multi-step electron transfer process, which has a slow reaction rate and high overpotential [9-12]. Therefore, exploring a kind of highly efficient electrocatalyst toward OER is of great importance. $RuO_2$ and $IrO_2$ are considered to be the best electrocatalysts for oxygen evolution reaction. While the limited reserves and expensive cost makes them not suitable to large-scale production for electrocatalytic reactions. Thus, it is significant to explore highly active and non-precious electrocatalysts [13-19].

With the valence electron structures of $3d^{6-8}4s^2$, the transition-metal (Fe, Co, Ni) oxides, hydroxides, and their alloys all exhibit excellent OER activity [20-25]. Also, people have found that metal molybdates ($MMoO_4$), as a family of functional materials, exhibit outstanding catalytic property in many fields, such as lithium-ion batteries (LIBs), supercapacitors and electrocatalysis due to the high oxidation state of molybdenum [26-28]. For instance, Zhang et al. reported that $FeMoO_4$ nanorods synthesized by one-step solvothermal method can be used as an electrocatalyst material with excellent properties [30]. Furthermore, some of these catalysts have to be immobilized on electrode surfaces using a polymer binder such as Nafion or PTFE, which are not conducive to active sites exposure, thereby increasing resistance and decreasing the catalytic activity. Therefore, the supported electrocatalysts may be the promising choice for high conductivity and dispersion [31-35].

In this work, nickel foam with a unique three-dimensional structure is used as the substrate to support $FeMoO_4$ nanoprism with rich defects and high intrinsic activity by a facile one-step hydrothermal method. Meanwhile, we explore the optimal ratio of molybdenum to iron to achieve the best OER performance. The results show that the $FeMoO_4$ nanoprism with the molar ratio of 1:1 ($n_{Mo}$:$n_{Fe}$) exhibits the best OER performance compared with those of contrastive catalysts, which only demands an overpotential of 284 mV to reach a current density of 100 mA $cm^{-2}$ in 1.0 M KOH.

## 2. EXPERIMENTAL SECTION

### *2.1 Chemicals and materials*

All reagents are of analytical grade and were used without further purification. Nickel foam (NF) was purchased from Kunshan Kuangxun Electrical Co,. Ltd. Sodium molybdat dihydrat ($Na_2MoO_4{\cdot}2H_2O$) and Iron (II) chloride tetrahydrate ($FeSO_4{\cdot}7H_2O$) were purchased from Sinopharm Chemical Reagent Co., Ltd. Deionized water (18.2 MΩ cm at 25 ℃) was used for experiments.

### *2.2 Preparation of NF based electrocatalysts*

The preparation of $FeMoO_4$-1 is as follows. Prior to use, the nickel foam (NF, 1×2 cm) was ultrasonically cleaned in dilute sulfuric acid, acetone and then ethanol for 30 min respectively. 1.0008 g of $FeSO_4{\cdot}7H_2O$ and 0.8710 g of $Na_2MoO_4{\cdot}2H_2O$ were dissolved in 45 ml of water under magnetic stirring for 15 min to form uniform solution. Then, the brown solution obtained above was transferred into a 100 mL Teflon-lined stainless steel autoclave. The washed NF was immersed into the above solution. Then, the autoclave was heated at 100 ℃ for 24 h. After cooling to 25 ℃ naturally, the NF was taken out and washed with water and ethanol several times and then dried at 60 ℃ for later use.

The same procedures were applied to obtain $FeMoO_4$-2 and $FeMoO_4$-3 by changing the amount of $Na_2MoO_4{\cdot}2H_2O$ to 0.4355 g and 1.3065 g, respectively.

The preparation of $FeO_x$ is similar to that of $FeMoO_4$-1 except that 1.0008 g of $FeSO_4{\cdot}7H_2O$ and 0.8710 g of $Na_2MoO_4{\cdot}2H_2O$ are replaced by 2.0016 g of $FeSO_4{\cdot}7H_2O$.

The preparation of $MoO_x$ is similar to that of $FeO_x$ except that 2.0016 g of $FeSO_4{\cdot}7H_2O$ is replaced by 1.7418 of $Na_2MoO_4{\cdot}2H_2O$.

*2.3 Characterization*

The crystal information was examined with X-ray diffraction (XRD) on X'Pert PRO MPD using Cu Kα with 2θ range from 10° to 90°. X-ray photoelectron spectra (XPS) measurements were conducted to study the chemical states of the constituent elements via a VG ESCALABMK II photoelectron spectrometer with Al Ka X-ray radiation as excitation source. Scanning electron microscopy (SEM) images (Hitachi S-4800) and high-resolution transmission electron microscopy (HRTEM) images (FEI Tecnai $G^2$, 200 kV) were conducted to reveal the microscopic morphology of the samples.

*2.4 Electrochemical measurements*

The electrocatalytic performances were investigated on a Gamry Reference 600 electrochemical workstation with a three-electrode system in 1.0 M KOH, using the NF based electrodes as the working electrode, platinum plate as the counter electrode, and saturated calomel electrode (SCE) as the reference electrode. The electrolyte of 1.0 M KOH was protected by $O_2$ during the process. All linear sweep voltammetry (LSV) polarization curves were recorded at a scan rate of 5 mV $s^{-1}$. Electrochemical impedance spectroscopy (EIS) data is performed with frequency from $10^5$ Hz to 0.1 Hz at an AC voltage of 0.4 V (vs. SCE). The electrochemical capacitance ($C_{dl}$) is determined by cyclic voltammograms (CVs) at increasing scan rates from 40 to 120 $mV \cdot s^{-1}$. The iR correction to data with the series resistance (Rs) is performed by $\eta_{corr} = \eta - iRs$. The potential conversion from SCE to RHE is based on the following equation: $E_{RHE} = E_{SCE} + 0.245 + 0.059 \times pH$.

## 3. RESULTS AND DISCUSSION

The XRD pattern of $FeMoO_4$ in Figure 1a shows a set of diffraction peaks at 13.0°, 23.0°, 26.2°, 32.5°, and 39.7°, corresponding to the (110), (021), (220), (022), and (330) planes of $FeMoO_4$ (PDF No. 00-022-0628) except for the peaks at 44.8°, 52.2° and 76.8° belonging to the NF substrate (PDF No. 00-003-1051). The $FeMoO_4$-2 and $FeMoO_4$-3 exhibit similar XRD patterns (Figure 1b), indicating that they are the same kind of $FeMoO_4$ only in different molar ratios. But the peak intensity of $FeMoO_4$-2 and $FeMoO_4$-3 are weaker than $FeMoO_4$-1, indicating $FeMoO_4$ prepared with the ratio of 1:1 ($n_{Mo}$:$n_{Fe}$) has higher purity and higher crystallinity than the molar ratio of 1:2 and 3:2. Therefore, we speculate the best ratio of Mo to Fe is 1:1.

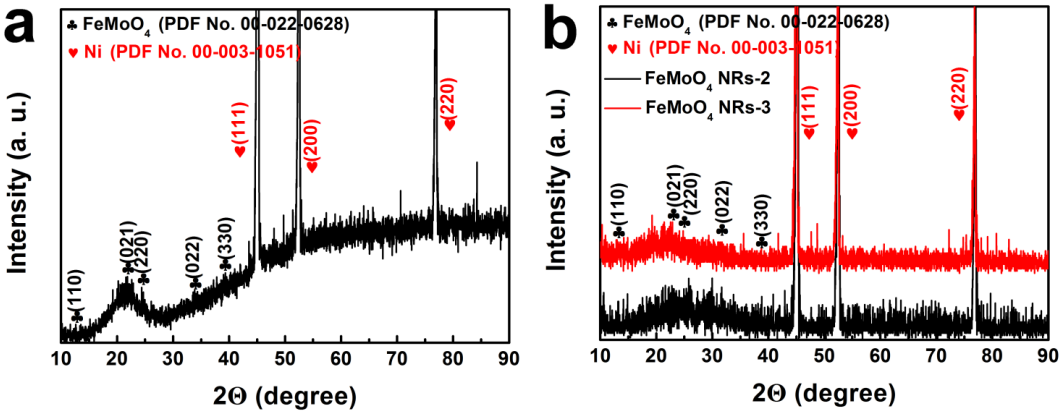


**Figure 1.** XRD patterns of (a) $FeMoO_4$-1, (b) $FeMoO_4$-2 and $FeMoO_4$-3.

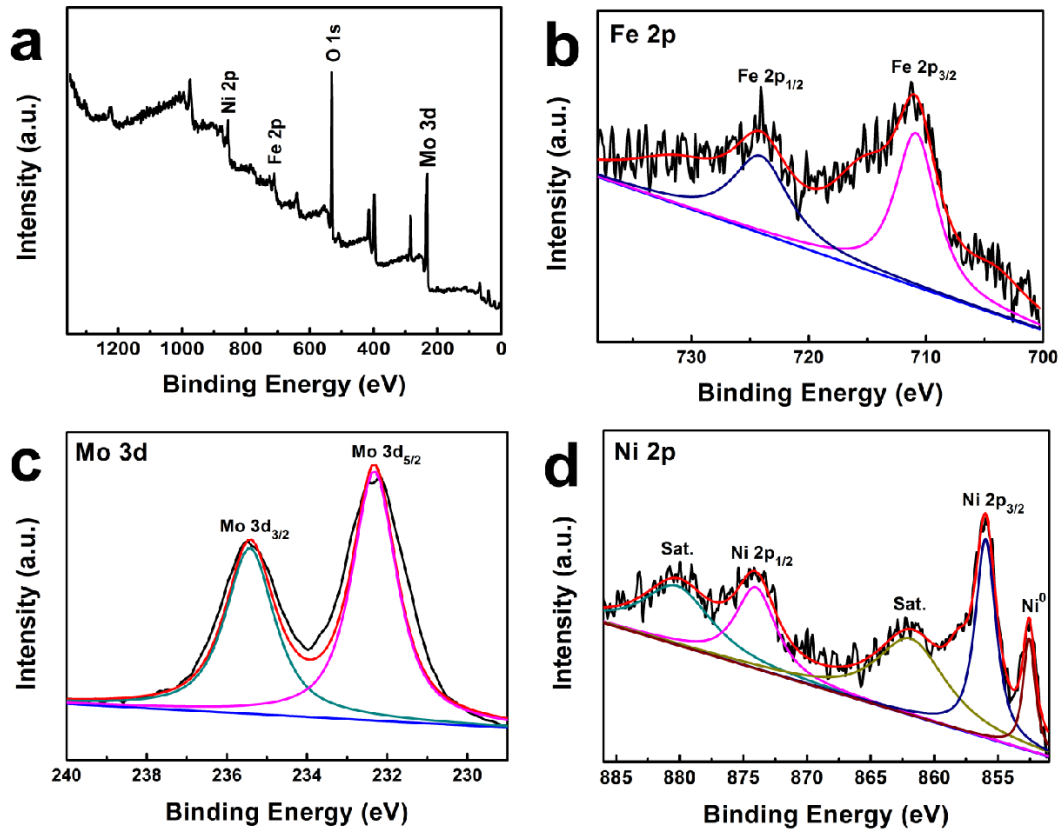


**Figure 2.** (a) Full XPS survey spectra of $FeMoO_4$-1, and XPS spectra of $FeMoO_4$-1 in the (b) Fe 2p; (c) Mo 3d and (d) Ni 2p regions

XPS measurement is further conducted to investigate the composition and valence state of $FeMoO_4$. $FeMoO_4$-1 was selected as the aimed electrocatalyst since it showes the best catalytic performances among all the prepared electrocatalysts (see detailed discussion below). As shown in Figure 2a, it shows that $FeMoO_4$ is composed of Fe, Mo, Ni and O as the major elements. From Figure 2b, the Fe 2p spectrum shows two peaks at 710.8 eV and 724.1 eV, which correspond to Fe $2p_{3/2}$ and Fe $2p_{1/2}$, respectively [36]. As shown in Figure 2c, two peaks located at 232.3 eV and 235.4 eV can be

assigned to Mo $3d_{5/2}$ and Mo $3d_{3/2}$, respectively, indicating the presence of high oxidation state of molybdenum, which is responsible for high catalytic activity [37]. Moreover, the XPS spectrum of Ni 2p (Figure 2d) show that binding energy peaks at 855.9 and 874.0 eV and associated satellite peaks at 861.8 and 880.2 eV, correspond to Ni $2p_{3/2}$ and Ni $2p_{1/2}$, respectively. Moreover, the peak located at 852.5 eV belongs to $Ni^0$. It is worth to note that element Ni derived from nickel foam can improve the conductivity and accelerate the diffusion of electrolytes and gas release.

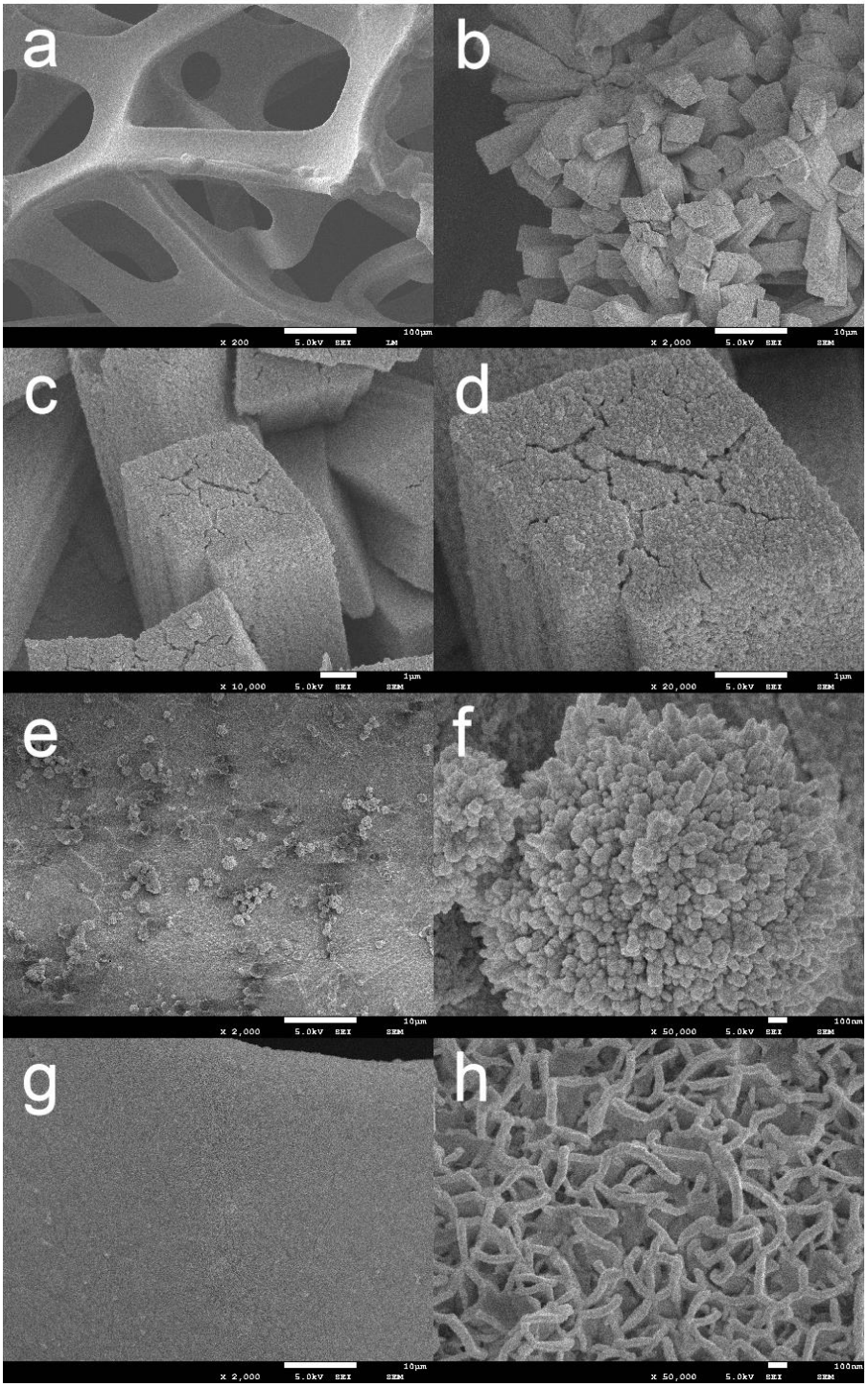


**Figure 3.** SEM images of (a) blank NF (b-d) $FeMoO_4$-1/NF (e, f) $FeO_x$/NF and (g, h) $MoO_x$/NF

The morphologies of blank NF, $FeMoO_4$-1, $FeO_x$ and $MoO_x$ are characterized by SEM (Fig 3). As shown in Figure 3a, blank NF with three-dimensional porous structure can expose active species and improve the conductivity. The SEM images of $FeMoO_4$-1 in Figure 3b-d reveal that a large number of uniform nanoprisms with an average length of 10 μm and diameter side length of 2.5 μm are formed. This unique structure provides excellent mass transfer channels for electrochemical catalytic processes and accelerate the transfer of electrons or ions. Figure 3e-f show many small balls are formed on the surface of $FeO_x$/NF, which are composed of sea urchin-like particles after being enlarged. Figure 3g-h show that uniform film composed of many vertical nanosheets with an average length of 200 nm is formed on the surface of $MoO_x$/NF.

HRTEM images of $FeMoO_4$-1 in Figure 4a-b also present prism-like morphology consistent with SEM results. As shown in Figure 4c, the edge of the prism is covered with rough film, which belongs to $FeMoO_4$. The loose structure facilitates the exposure of the active sites, thereby improving the catalytic performance of oxygen evolution reaction. In Figure 4d, the marked lattice fringe with d-spacing of 0.34 nm agrees well with the (220) plane of $FeMoO_4$ nanoprism. All of these characterizations demonstrate the successful preparation of $FeMoO_4$/NF nanoprism.

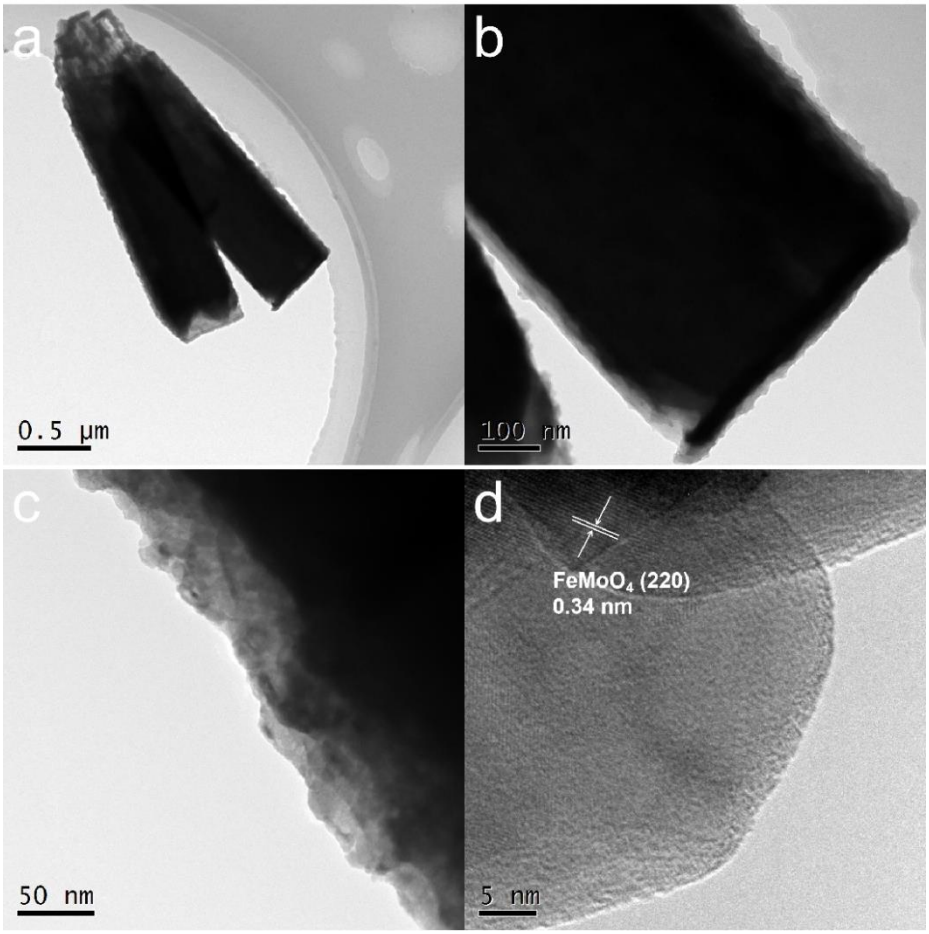


**Figure 4.** HRTEM images of (a-d) $FeMoO_4$-1/NF

The electrocatalytic activities of blank NF, $FeMoO_4$-1, $FeMoO_4$-2, $FeMoO_4$-3, $FeO_x$ and $MoO_x$ toward OER are investigated in 1.0 M KOH. LSV curves are first discussed in Figure 5a. Among the three $FeMoO_4$/NF electrodes of different ratios of Mo to Fe, the $FeMoO_4$-1 exhibits the highest OER activity with a lowest overpotential of 284 mV to reach 100 mA $cm^{-2}$ as compared to 292 and 286 mV achieved by the $FeMoO_4$-2 and $FeMoO_4$-3 electrodes, respectively. The results demonstrate the advantage of nanoprism structure. It is worth to note that $FeMoO_4$-1 is also superior to other reported non-noble-metal electrocatalysts to reach 100 mA $cm^{-2}$ in 1.0 M KOH, including $FeSe_2$/NF (308 mV) [37] and $Ni_3S_2$/NF (450 mV) [40]. Table 1 gives a more detailed comparison. In addition, Tafel plots in Figure 5b are obtained by Tafel equation ($\eta = b \log j + a$) to evaluate OER kinetics. Again, the $FeMoO_4$-1 electrode achieves the lowest Tafel plot of 62.66 mV $dec^{-1}$, with the $FeMoO_4$-3 electrode (72.36 mV $dec^{-1}$) coming next, followed by the $FeMoO_4$-2 electrode (85.87 mV $dec^{-1}$), indicating that the $FeMoO_4$-1 electrode has a fast kinetics for OER in 1.0 M KOH. Electrochemical impedance spectroscopy (EIS) was used to evaluate the charge transfer resistance of the sample electrode during OER process. As displayed in Figure 5c, the resulting Nyquist plots indicate that the $FeMoO_4$-1 electrode with the smallest semicircle has the smallest charge transfer resistance than $FeMoO_4$-2, $FeMoO_4$-3, $FeO_x$ and $MoO_x$. Furthermore, electrochemically active surface area (ECSA) is another important factor influencing the catalytic performance. The double layer capacitances ($C_{dl}$) are applied to estimate ECSAs of catalysts using CVs at 40, 60, 80, 100 and 120 mV $s^{-1}$. As displayed in Figure 5d, $FeMoO_4$-1/NF possesses the largest $C_{dl}$ value (12.05 mF $cm^{-2}$), consistent with the conclusion drawn from the overpotential, Tafel slope and Nyquist plots.

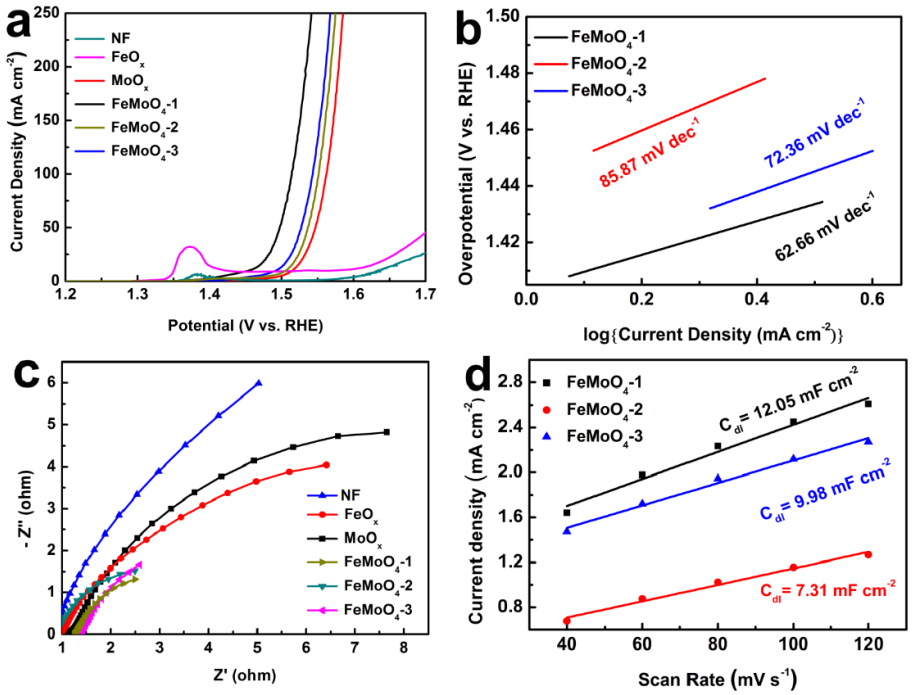


**Figure 5**. (a) LSV curves of blank NF, $FeO_x$/NF, $MoO_x$/NF, $FeMoO_4$-1/NF, $FeMoO_4$-2/NF and $FeMoO_4$-3/NF recorded in 1.0 M KOH at a scan rate of 5 mV $s^{-1}$ and corresponding (b) Tafel plots and (c) Nyquist plots. (d) Plots of current density difference against scan rate for calculation of double layer capacitance ($C_{dl}$).

**Table 1.** Comparison of OER performance with other non-noble-metal electrocatalysts in 1.0 M KOH.

| **Catalyst** | ***J* (mA cm$^{-2}$)** | **Voltage (mV)** | **Ref.** |
|---|---|---|---|
| $FeMoO_4$-1/NF | **100** | **284** | **This work** |
| $NiCo_2O_4$@$CoMoO_4$/NF-7 | 20 | 265 | 38 |
| $FeSe_2$/NF | 100 | 308 | 39 |
| FeOOH(Se)/IF | 100 | 364 | 40 |
| $FeB_2$ | 100 | 410 | 41 |
| $Ni_3S_2$/NF | 100 | 450 | 42 |
| CoFe/NF | 10 | 220 | 43 |
| $NiCo_2O_4$ | 10 | 290 | 44 |
| $CuCo_2O_4$/NrGO | 10 | 360 | 45 |
| β-$NiMoO_4$ | 10 | 300 | 46 |
| $CoMoO_4$ | 10 | 343 | 47 |

## 4. CONLUSIONS

In summary, highly efficient electrocatalysts have been developed by in-situ growth of $FeMoO_4$ nanoprism on nickel foam through a simple one-step hydrothermal method. The electrochemical measurements suggest that the $FeMoO_4$-1/NF electrode is a promising oxygen evolution reaction catalyst in alkaline solution. Compared with single metal oxides, the $FeMoO_4$-1/NF with a molar ratio of 1:1 ($n_{Mo}$:$n_{Fe}$) demonstrates the enhanced activity for OER with a small overpotential of 284 mV to reach 100 mA cm$^{-2}$. Our work provides the promising way for designing bimetallic material as excellent OER electrocatalysts.

## References

1. M. Li, X. Tu, Y. Wang, Y. Su, J. Hu, B. Cai, J. Lu, Z. Yang, Y. Zhang, *Nano-Micro Letters*, 10 (2018) 45.
2. X. Shang, J.Q. Chi, S.S. Lu, B. Dong, X. Li, Y.R. Liu, K.L. Yan, W.K. Gao, Y.M. Chai, Y.Q. Liu, C.G. Liu, *Int. J. Hydrogen Energy*, 42 (2017) 4165.
3. C. F. Du, Q. Liang, R. Dangol, J. Zhao, H. Ren, S. Madhavi, Q. Yan, *Nano-Micro Letters*, 10 (2018) 67.

4. C. Tang, H. F. Wang, Q. Zhang, *Acc. Chem. Res.*, 51 (2018) 881.
5. X.Y. Zhang, B.Y. Guo, Q.W. Chen, B. Dong, J.Q. Zhang, J.F. Qin, J.Y. Xie, M. Yang, L. Wang, Y.M. Chai, C.G. Liu, *Inter. J. Hydrogen Energy*, 44 (2019) 14908.
6. Y. Yu, Y. Shi, B. Zhang, *Acc. Chem. Res.,* 51 (2018) 1711.
7. Q. Wang, L. Shang, R. Shi, X. Zhang, Y. Zhao, G. I. N. Waterhouse, L. Z. Wu, C. H. Tung, T. Zhang, *Adv. Energy Mater.*, 7 (2017) 1700467.
8. X. Shang, K. L. Yan, Y. Rao, B. Dong, J. Q. Chi, Y. R. Liu, X. Li, Y. M. Chai, C. G. Liu, *Nanoscale*, 9 (2017)12353.
9. Z. J. Xu, *Nano-Micro Letters*, 10 (2018) 8.
10. Y. Guo, J. Zhang, P. Yuan, M. Zhou, J. Li, Y. Qiao, S. Mu, Q. Xu, *Advanced Functional Materials*, 28 (2018) 1805641.
11. J. Wei, M. Zhou, A. Long, Y. Xue, H. Liao, C. Wei, Z. J. Xu, *Nano-Micro Letters*, 10 (2018) 75.
12. Y. M. Chai, X. Y. Zhang, J. H. Lin, J. F. Qin, Z. Z. Liu, J. Y. Xie, B. Y. Guo, Z. Yang, B. Dong, *Inter. J. Hydrogen Energy*, 44 (2019) 10156.
13. Z. Cai, D. Zhou, M. Wang, S. M. Bak, Y. Wu, Z. Wu, Y. Tian, X. Xiong, Y. Li, W. Liu, S. Siahrostami, Y. Kuang, X. Q. Yang, H. Duan, Z. Feng, H. Wang, X. Sun, *Angew. Chem. Int. Ed.,* 57 (2018) 9392.
14. Q. Yue, C. Liu, Y. Wan, X. Wu, Xi. Zhang, P. Du, *J. Catal.*, 358 (2018) 1.
15. X. F. Lu, L. F. Gu, J. W. Wang, J. X. Wu, P. Q. Liao, G. R. Li, *Adv. Mater.*, 29 (2017) 1604437.
16. D. Chen, M. Qiao, Y. R. Liu, L. Hao, D. Liu, C. L. Dong, Y. Li, S. Wang, *Angew. Chem. Int. Ed.,* 57 (2018) 8691.
17. Y. Pi, Q. Shao, P. Wang, F. Lv, S. Guo, J. Guo, X. Huang, *Angew. Chem. Int. Ed.*, 56 (2017) 4502.
18. Y. Li, F. M. Li, X. Y. Meng, S. N. Li, J. H. Zeng, Y. Chen, *ACS Catal.*, 8 (2018) 1913.
19. Z. Yan, H. Sun, X. Chen, H. Liu, Y. Zhao, H. Li, W. Xie, F. Cheng, J. Chen, *Nat. Commun.*, 9 (2018) 2373.
20. X. Chia, M. Pumera, *Nature Catalysis*, 1 (2018) 909.
21. X. Yang, J. Chen, Y. Chen, P. Feng, H. Lai, J. Li, X. Luo, *Nano-Micro Letters*, 10 (2018) 15.
22. K. L. Yan, J. Q. Chi, Z. Z. Liu, B. Dong, S. S. Lu, X. Shang, W. K. Gao, Y. M. Chai, C. G. Liu, *Inorganic Chemistry Frontiers*, 4 (2017) 1783.
23. B. Han, M. Risch, S. Belden, S. Lee, D. Bayer, E. Mutoro, Y. Shao-Horn, *J. Electrochem. Soc.*, 165 (2018) F813.
24. Y. Yang, L. Dang, M. J. Shearer, H. Sheng, W. Li, J. Chen, P. Xiao, Y. Zhang, R. J. Hamers, S. Jin, *Advanced Energy Materials*, 8 (2018) 1703189.
25. M. Asnavandi, Y. Yin, Y. Li, C. Sun, C. Zhao, *ACS Energy Letter*, 3 (2018) 1515.
26. H. Zhang, C. Lu, H. Hou, Y. Ma, S. Yuan, *Chem. Eng. J.,* 370 (2019) 400.
27. Y. R. Liu, X. Shang, W. K. Gao, B. Dong, X. Li, X. H. Li, J. C. Zhao, Y. M. Chai, Y. Q. Liu, C. G. Liu, *J. Mater. Chem. A*, 5 (2017) 2885.
28. C. Liang, Y. Tao, N. Yang, D. Huang, S. Li, K. Han, Y. Luo, H. Chen, L. Mai, *Electrochimica Acta*, 311 (2019) 192.
29. X. Zhao, J. Meng, Z. Yan, F. Cheng, J. Chen, *Chinese Chemical Letters*, 30 (2019) 319.
30. Y. Zhang, W. Y. Li, T. W. Ng, W. P. Kang, C. S. Lee, W. J. Zhang, *J. Mater. Chem. A*, 3 (2015) 20527.
31. X. Shang, X. Li, W. H. Hu, B. Dong, Y. R. Liu, G. Q. Han, Y. M. Chai, Y. Q. Liu, C. G. Liu, *Appl. Surf. Sci.*, 378 (2016) 15.
32. J. Li, W. Xu, J. Luo, D. Zhou, D. Zhang, L. Wei, P. Xu, D. Yuan, *Nano-Micro Letters*, 10 (2018) 6.
33. X. Li, K. L. Yan, Y. Rao, B. Dong, X. Shang, G. Q. Han, J. Q. Chi, W. H. Hu, Y. R. Liu, Y. M. Chai, C. G. Liu, *Electrochimica Acta*, 220 (2016) 536.
34. L. L. Feng, G. Yu, Y. Wu, G. D. Li, H. Li, Y. Sun, T. Asefa, W. Chen, X. X. Zou, *J. Am. Chem. Soc.,* 137 (2015) 14023.
35. B. You, X. Liu, G. Hu, S. Gul, J. Yano, D. Jiang, Y. Sun, *J. Am. Chem. Soc.*, 139 (2017) 12283.

36. Z. Zhang, C. Hua, M. Hashima, P. Chenb, Y. Xiong, C. Zhang, *Mater. Sci. Eng., B*, 176 (2011) 756.
37. X. Wu, J. Du, H. Li, M. Zhang, B. Xi, H. Fan, Y. Zhu, Y. Qian, *J. Solid State Chem.*, 180 (2007) 3288.
38. Y. Q. Gong, Z. Yang, Y. Lin, J. L. Wang, H. L. Pan, Z. F. Xu, *J. Mater. Chem. A*, 6 (2018) 16950.
39. C. Panda, P. W. Menezes, C. Walter, S. L. Yao, M. E. Miehlich, V. Gutkin, K. Meyer, M. Driess, *Angew. Chem. Int. Ed.*, 56 (2017) 1056.
40. S. Niu, W. J. Jiang, Z. X. Wei, T. Tang, J. M. Ma, J. S. Hu, L. J. Wan, *J. Am. Chem. Soc.*, 29 (2019) 1701584.
41. H. Li, P. Wen, Q. Li, C. C. Dun, J. H. Xing, C. Lu, S. Adhikari, L. Jiang, D. L. Carroll, S. M. Geyer, *Adv. Energy. Mater.*, 7 (2017) 1700513.
42. X. Zou, Y. P. Liu, G. D. Li, Y. Y. Wu, D. P. Liu, W. Li, H. W. Li, D. J. Wang, Y. Zhang, X. X. Zou, *Adv. Mater.*, 29 (2017) 1700404.
43. P. Babar, A. Lokhande, H. H. Shin, B. Pawar, M. G. Gang, S. Pawar, J. H. Kim, *Small*, 14 (2018) 1702568.
44. X. H. Gao, H. X. Zhang, Q. G. Li, X. G. Yu, Z. L. Hong, X. W. Zhang, C. D. Liang, Z. Lin, *Angew. Chem. Int. Ed.*, 55 (2016) 6290.
45. S. K. Bikkarolla, P. Papakonstantinou, *J. Power Sources*, 281 (2015) 243.
46. S. Ratha, A. K. Samantara, K. K. Singha, A. S. Gangan, B. Chakraborty, B. K. Jena, C. S. Rout, *ACS Appl. Mater. Interfaces*, 9 (2017) 9640.
47. X. Liu, Y. Yang, S. Guan, Chem. *Phys. Lett.*, 675 (2017) 11.